Thickness Dependence in Phase Formation and Properties of TaSe2 Layers Grown on GaP(111)B

Corentin Sthioul, Yevheniia Chernukha, Houda Koussir, Christophe Coinon, Gilles Patriarche, David Troadec, Louis Thomas, Pascal Roussel, Bruno Grandidier, Pascale Diener, et al.

Thickness dependence in phase formation and properties of $TaSe_2$ layers grown on $GaP(111)_B$

Corentin Sthioul,*,† Yevheniia Chernukha,† Houda Koussir,† Christophe Coinon,† Gilles Patriarche,‡ David Troadec,† Louis Thomas,† Pascal Roussel,¶ Bruno Grandidier,† Pascale Diener,† and Xavier Wallart†

†*Univ. Lille, CNRS, Centrale Lille, Univ. Polytechnique Hauts-de-France, Junia-ISEN, UMR 8520 - IEMN, F-59000 Lille, France*

‡*Univ. Paris-Saclay, CNRS, Centre de Nanosciences et de Nanotechnologies, 91120 Palaiseau, Paris, France*

¶*Unité de Catalyse et de Chimie du Solide (UCCS), Univ. Lille, CNRS, Centrale Lille, Univ. d'Artois, UMR 8181 - UCCS, F-59000 Lille, France*

E-mail: corentin.sthioul@univ-lille.fr

Abstract

The effect of growth temperature and subsequent annealing on the epitaxy of both single and few layers $TaSe_2$ on Se-terminated $GaP(111)_B$ substrates is investigated. The selective growth of the 1T and 1H phases is shown up to 1 ML according to X-ray and ultraviolet photoelectron spectroscopies. The 1H monolayer, favored at low temperature, exhibits a very homogeneous coverage after annealing, while the 1T ML, grown at high temperature, is characterized by a better in-plane orientation. Moreover, X-ray photoelectron diffraction spectroscopy performed on 1T submonolayers shows a

negligible amount of mirror twins. By contrast, in multilayers, scanning transmission electron microscopy always reveals a mixture of $2H_a$ and 3R polytypes with very few 1T. In addition, the multilayers become Se-deficient above 500°C and a new interfacial phase identified as $Ta_{1+x}Se_2$ or TaP appears. Finally, the optimized multilayers grown between 250 and 500°C exhibits a similar metallic behavior with a resistivity comparable to the bulk one with valuable outcomes in the formation of electrical contacts for 2D-material based devices.

Keywords

Transition metal dichalcogenide, molecular beam epitaxy, tantalum diselenide, gallium phosphide, X-ray photoelectron spectroscopy, scanning transmission electron microscopy, atomic force microscopy

1 Introduction

Layered transition metal dichalcogenides (TMDCs) are a family of two-dimensional materials of chemical formula MX_2 where M is a transition metal (Ti, Zr, Nb, Ta, Mo, W...) and X a chalcogen (S, Se or Te). The metal atom is covalently bounded to 2 chalcogens to form monolayers (MLs) of 3 atomic planes, which are sticked together by weak Van der Waals (vdW) forces. The large variety of compounds and structures they form covers a wide range of properties and possible applications.[1]

Among them, group V TMDCs (VX_2, NbX_2 and TaX_2) are metallic and can be used as low-resistance contact for TMDC-based devices.[2–4] They also exhibit charge density waves (CDW), superconductivity (SC) and Mott insulator states.[5] All these properties are found in $TaSe_2$ thanks to the rich diversity of phases. In monolayer, Ta atoms can be either in octahedral coordination in the 1T phase, or in trigonal prismatic coordination in the 1H phase. Different stacking sequences of 1H MLs lead to $2H_a$, 3R and $4H_a$ phases, while $4H_b$

and 6R-$TaSe_2$ consist in stackings of both 1T and 1H MLs.[6] 1T-$TaSe_2$ has been by far the most studied because its $\sqrt{13}\times\sqrt{13}$ CDW is commensurate up to 473 K[7] and it is also a Mott insulator at room temperature in monolayer.[8] These remarquably high temperature CDW or Mott-insulating states may be a key for the developpement of memory devices operating at room temperature, following the demonstration of a nonvolatile resistive switching in 1T-TaS_2,[9] a similar material. By contrast, the $2H_a$ phase remains metallic and has CDW transitions only below 122 K[10] and SC below 0.14 K.[11] The critical temperature for SC is higher in 3R[12] and $4H_a$-$TaSe_2$,[13] but it is also increased by doping,[14] alloying,[15] with Ta self-intercalation[16] and random layer stacking.[17] Still, because doping and non-stoichiometry are also promoting phase change[16,18] and disorder,[17,19] the origin of SC has been debated as well as its interplay with the weakening of the CDW.[14,20]

Most of these studies were performed on crystals grown by chemical vapour transport (CVT) and exfoliated flakes. Because they require transfer processes incompatible with scalable device fabrication, efforts have been recently made to achieve wafer-scale coverage with chemical vapor deposition (CVD).[21] But this technique requires too high growth temperatures to be compatible with many substrates and chip manufacturing processes. By contrast, molecular beam epitaxy (MBE) is known to grow wafer scale TMDCs, free of contamination and with high control of the thickness, despite smaller grain size because of reduced growth temperatures. Many substrates have been used for $TaSe_2$ growth, including MoS_2, $MoTe_2$, and $SnSe_2$,[22] GaAs,[23] AlN, $MoSe_2$ and $HfSe_2$,[24] Al_2O_3 and SiC[16] for few-layers, and graphene[25,26] for monolayer. Among the 3D substrates, III-V semiconductors are promising thanks to the passivation of their surface by Se atoms as demonstrated on GaAs,[27] which makes them suitable for vdW epitaxy. However, the single study on $TaSe_2$ grown on GaAs reported a mixture of several polytypes at every temperature, with the octahedrally coordinated layers (1T-like) only observed at low temperature,[23] in contradiction to the phase formation on graphene.[25,26] Owing to a larger temperature stability than GaAs,[28,29] GaP substrates should enable the exploration of higher growth temperatures. A first result has

demonstrated the successful growth of a good quality 1T-$TaSe_2$ monolayer on GaP.[30]

In this article, we show that the formation of the 1T or 1H phase in monolayer can be controlled through the growth temperature. By contrast, the H polytypes ($2H_a$, 3R) are always dominant in multilayers, pointing toward an effect of the thickness in the phase stability. The lowest surface roughness is obtained at low growth temperatures while the crystallinity and in-plane orientation are improved at high temperatures. However, too high temperatures lead to the formation of an interfacial compound and a Se-deficient $TaSe_2$ layer. The electrical characterization of the optimized multilayers finally demonstrates a resistivity similar to bulk and suggests a possible use as high work function metal electrodes for 2D TMDC heterostructures.

2 Experimental section

$GaP(111)_B$ substrates were deoxidized in a III-V MBE chamber under atomic H and cracked PH_3 up to 540°C. They were kept under vacuum during the transfer to another MBE chamber dedicated to selenide compounds. High purity Ta was evaporated using an e-beam evaporator and Se_x molecules from a Riber VCOR 110 effusion cell with a 425°C cracking zone. Se and Ta flux were measured using a quartz crystal microbalance. To ensure a large excess of chalcogen, the Se/Ta ratio was kept larger than 100 and the Ta flux was chosen to achieve a growth rate in the range 0.005-0.007 Å/s (3-4 ML/h). The growth was monitored in-situ by reflection high-energy electron diffraction (RHEED) and the temperatures were measured using a pyrometer calibrated against the InSb melting point at 525°C, or a thermocouple below 350°C. When the samples were annealed, the temperature was increased at a constant rate of 20°C/min and maintained 3 minutes under Se flux, then cooled rapidly.

The samples were transferred under vacuum to an analysis chamber fitted with a Physical Electronics 5600 system for X-ray photoelectron spectroscopy (XPS), Ultraviolet photoelectron spectroscopy (UPS) and low-energy electron diffraction (LEED) characterizations. XPS

was performed with a monochromatic Al K_α anode (1486.6 eV) making a 90° angle with the hemispheric photoelectron analyzer whose acceptance angle was set to 14°. For X-ray photoelectron diffraction (XPD) experiments, a Mg K_α anode was used (1253.6 eV) and the analyzer acceptance angle reduced to 4°. In UPS, the valence band spectra were recorded around the Γ point of the Brillouin zone with the HeI radiation (21.2 eV) generated by a He plasma UV source. XPS measurements were used to check that the layers were free of contamination and had comparable thicknesses. For quantitative XPS measurements, the intensity was normalized by photoelectric cross-sections determined by Scofield[31] and corrected by the asymmetry parameter from Yeh[32] and the electron effective attenuation lengths from the NIST database.[33] An estimation of the thickness was deduced from the Ta $4f$ and Ga $3d$ CLs originating from the layer and the substrate respectively.[34] As $TaSe_2$ is expected to be metallic, the binding energy scale of all UPS and XPS spectra have been shifted in order to have the Fermi level at 0 eV. In 1T-$TaSe_2$ monolayers, the Mott gap (0.13 eV[30]) is too small to be resolved at room temperature and the correct calibration of the binding energy is verified by the position of the lower Hubbard band at 0.2 eV.[25]

Before grazing incidence X-ray diffraction (GIXRD), scanning transmission electron microscopy (STEM) and electrical measurements, the $TaSe_2$ layers were protected from oxidation by a 30-50 nm-thick amorphous selenium capping layer deposited at a substrate temperature below 20°C. In-plane GIXRD measurements were carried out using a SmartLab Rigaku diffractometer equipped with a 9 kW Cu rotated anode (K_α $\lambda = 1.5418$ Å) collimated by 0.114° slits. STEM studies were performed in a Titan Themis 200 (FEI) microscope equipped with a spherical aberration corrector on the probe and an energy-dispersive x-ray spectroscopy (EDX) system super X (0.7 srad solid angle of collection). The accelerating voltage was 200 kV. The (half) convergence angle of the probe is 17.6 mrad and the probe current 40-45 pA. The inner and outer semi-angles of the Dark Field detector are respectively 69 mrad and 200 mrad, detecting inelastically scattered electrons at high angles (HAADF-STEM images).

Atomic force microscopy (AFM) images were scanned in tapping mode using a Dimension D3100 microscope and NCHV-A probes from Bruker. The samples were exposed to ambient conditions for less than 12h before and during AFM measurements. The images were processed using the Gwyddion software to remove typical artifacts and calculate statistical quantities.[35]

3 Results and discussion

3.1 Growth of $TaSe_2$ monolayers

To explore the influence of the substrate temperature, $TaSe_2$ monolayers were grown at 250 450, 550 and 600°C. The RHEED patterns of the as-grown samples are presented Fig. 1 (a-d). All samples verify the epitaxial relationships in-plane $TaSe_2\,[1\,0\,\bar{1}\,0] \parallel [2\,\bar{1}\,\bar{1}]$ GaP and $TaSe_2\,[1\,1\,\bar{2}\,0] \parallel [1\,\bar{1}\,0]$ GaP and out-of-plane $TaSe_2\,[0\,0\,0\,1] \parallel [\bar{1}\,\bar{1}\,\bar{1}]$ GaP. The diffuse RHEED patterns at low temperatures denote a poorly crystalline material. It is in line with the observation of very small domains on the sample grown at 250°C by AFM (Supplementary 1). On the other hand, the extra spots at higher temperatures indicate increased surface roughness.

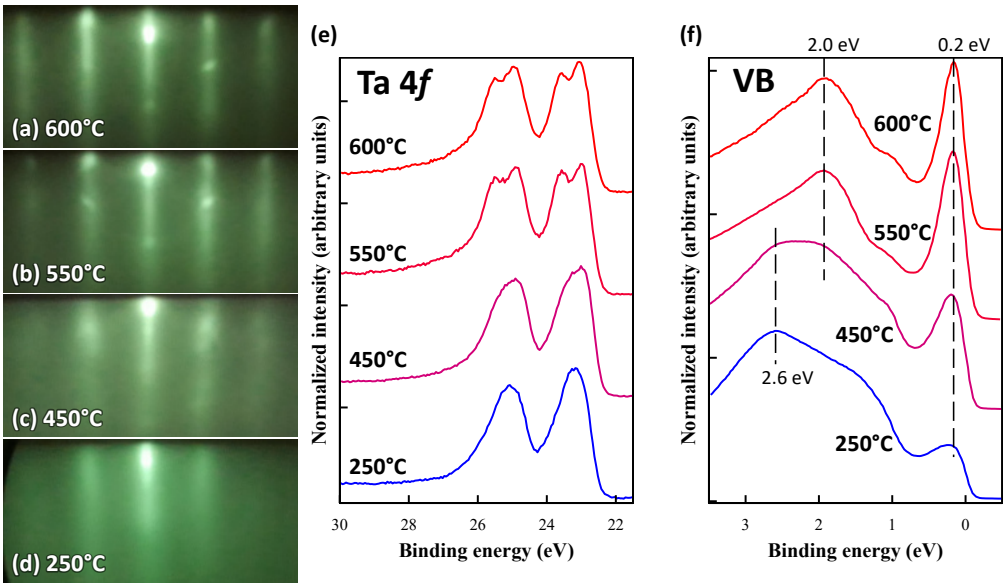

Figure 1: RHEED pattern along a $[1\,0\,\bar{1}\,0]$ direction of the $TaSe_2$ layers grown at (a) 600°C, (b) 550°C, (c) 450°C and (d) 250°C. (e) Corresponding XPS spectra of Ta $4f$ CLs measured at an emission angle of 45°. (f) Corresponding valence band measured in UPS at a take-off angle of 90°. XPS and UPS spectra were normalized and vertically shifted for clarity.

The XPS characterization of the layers (Fig. 1 (e)) reveals an evolution of the Ta $4f$ core level lines (CLs) from a large doublet to a split doublet with increasing growth temperatures. Both are asymmetric as expected for a metallic material. The splitting can be attributed to the CDW of the 1T phase,[36] as shown by the peak decompositions (Supplementary 2) for the samples grown at 550°C and 600°C. Moreover, the valence band measured around Γ by UPS and presented Fig. 1 (f) shows an increase of the electron density around 0.2 eV below the Fermi energy (E_F) with increasing temperatures. It is compatible with the previous observation of a large flat band in 1T-$TaSe_2$ attributed to the lower Hubbard band[25] and agrees with the phase evolution observed with XPS. As the XPS and UPS spectra for the samples grown at 550°C and 600°C are very similar, the 1T phase is already dominant at 550°C. Conversely, a low electron density near E_F is observed in the sample grown at 250°C. As band structure calculations predict the half-filled Ta $5d$ orbitals to be above the Fermi level at the Γ point in 1H-$TaSe_2$,[25,37] this smaller peak is attributed to the presence of a minority of 1T phase among a predominant 1H phase. At higher binding energies, the

maximum of the valence band is located at 2.6 eV for the sample grown at 250°C and shifts at 2 eV for the samples grown at 550°C and 600°C. If we assign these peaks to the 1H and 1T phases respectively, it is likely that both are present on the sample grown at 450°C making the valence band almost flat between 2.0 and 2.5 eV. This temperature appears thus as the transition temperature between both phases. Compared to previous results on graphene, these observations are more in line with a 1H/1T phase transition at 490°C[25] rather than at 600°C,[26] although the substrate may also play a role.

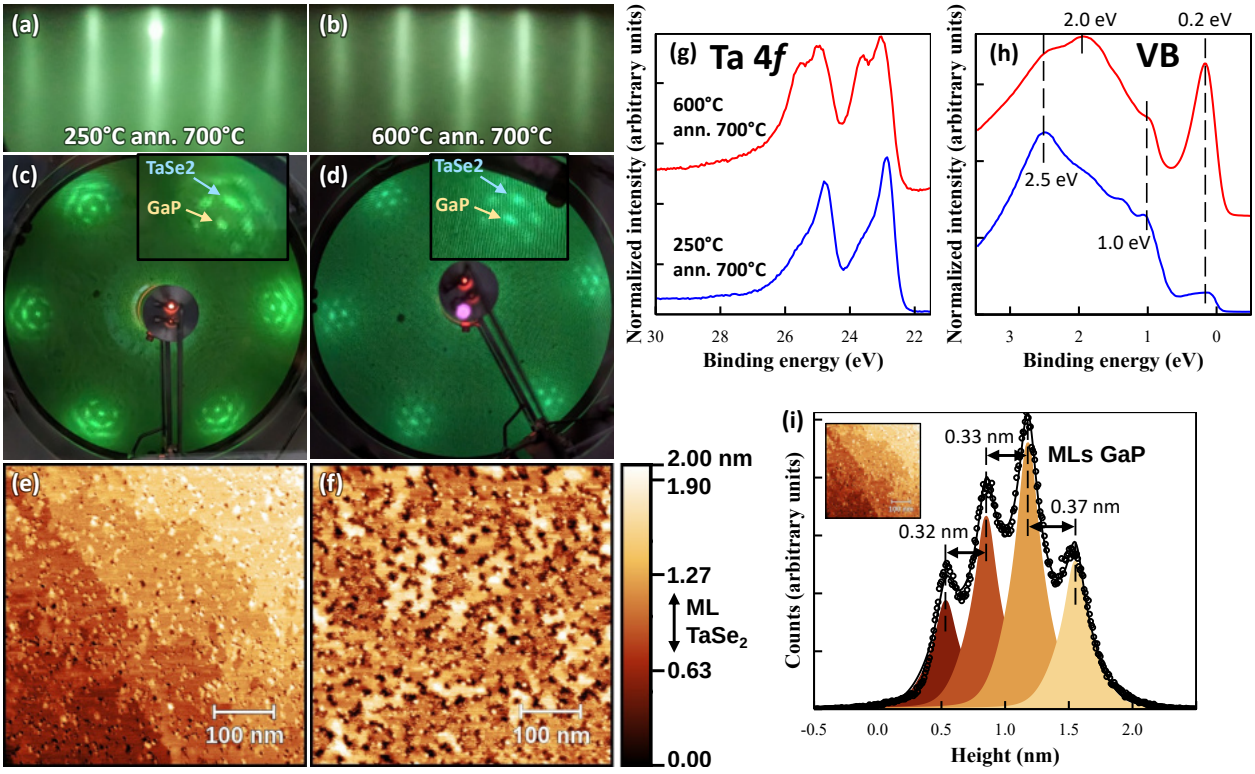

Figure 2: RHEED patterns along a $[1\,0\,\bar{1}\,0]$ direction of the $TaSe_2$ monolayers grown at 250°C and 600°C after annealing at 700°C (a-b). Corresponding LEED patterns (c-d), AFM images (e-f), XPS spectra of the Ta $4f$ CLs measured at a take-off angle of 45° (g) and valence band measured in UPS (h). The XPS and UPS spectra have been vertically shifted for clarity. (i) Histogram of the atomic step height measured in the AFM image (e), fitted using pseudo-Voigt functions. The LEED image (d) is reproduced from.[30] Copyright 2023 American Chemical Society.

To improve the quality and morphology of both 1H and 1T monolayers, samples grown at 250°C and 600°C have been annealed for 3 minutes at 700°C under a Se flux. The RHEED pattern of the 250°C-grown sample has become more resolved and brighter. Similarly, for

the 600°C-grown sample, a structural improvement is also seen as the spots have almost vanished. As shown in Fig. 2 (a-b), both patterns now exhibit thin streaks as expected for an epitaxial 2D layer. Moreover, in the LEED diagrams (Fig. 2 (c-d)), a moiré pattern is clearly visible. As discussed elsewhere,[30] its observation confirms the relaxation of the $TaSe_2$ lattice which occurs in vdW epitaxy to maintain the epitaxial registry with the GaP substrate. The $TaSe_2$ diffraction spots of the layer grown at 250°C (Fig. 2 (c)) are slightly enlarged compared to those of the 600°C-grown sample. This effect is attributed to a larger in-plane misorientation. In agreement with the RHEED observations, the AFM image of the sample grown at 250°C (Fig. 2 (e)) reveals a surface of good quality with flat terraces. The latter originate from the GaP substrate according to the measured step height of 0.35 nm (expected 0.315 nm[38]) on the histogram (Fig. 2 (i)). We attribute the small deviation of the height from the theoretical value to the drift of the AFM scanner during the acquisition of the image. The number of clusters and depressions on the different terraces is small, signature of a homogeneous coverage after annealing. By contrast, the substrate atomic steps are not visible on the layer grown at 600°C (Fig. 2 (f)) due to an increased roughness arising from 2 ML-thick islands and uncovered areas. Approximately 20 nm-wide and 100 nm-long $TaSe_2$ domains are obtained, whose continuity has been checked by scanning tunneling microscopy (Supplementary 3).

XPS and UPS spectra of the annealed layers presented respectively in Fig. 2 (g) and (h) reveal very little changes for the sample grown at 600°C. The Ta $4f$ lines and the valence band edges do not show any strong modification. In the latter spectrum, we note two small changes induced by the annealing: the shape of the spectrum around 1 eV is slightly different and a shoulder is visible at 2.5 eV, suggesting the formation of a minor fraction of 1H phase. Conversely, the annealing of the sample grown at 250°C leads to more significant changes of the spectra. The Ta $4f$ CLs are now very narrow with a characteristic shoulder that was previously reported for the bulk 2H phase.[39] The UPS spectra around Γ also exhibits distinct bands at 1.0 and 1.3 eV in addition to the one at 2.5 eV. These are certainly related

to the improvement of the crystalline quality, possibly along with a greater purity of the 1H phase.

Finally, even if the 1T phase is formed at high temperatures, the annealing at 700°C of a sample grown at low temperature does not result in the transformation of the 1H phase into the 1T phase. Conversely, the annealing of the 1T layer, grown at high temperature, leads to the formation of a small fraction of the 1H phase. It highlights the metastable nature of the 1T phase, well documented in bulk,[40] which could make its preparation more challenging. Nevertheless, our results demonstrate the possibility to selectively grow both 1H and 1T-$TaSe_2$ monolayers on GaP.

3.2 First stage of $TaSe_2$ growth

The alignment of the $TaSe_2$ layers along the crystallographic directions of the substrate has been shown through LEED and RHEED. Diffraction patterns are, in a first approximation,[41] symmetrical and produces 6 spots even though TMDCs have only 3-fold symmetry. Therefore, two non-equivalent orientations of a TMDC are nearly indistinguishable with these techniques. Because the nucleation density is generally important in TMDCs grown by MBE, it is of significant interest to get only one orientation to enable the grain coalescence and avoid mirror twin defects.[42] Unlike graphene, GaP has a 3-fold symmetry hence the two mirror orientations are expected to have different energies so one may be predominant.

To answer this question, 0.3 ML-thick $TaSe_2$ layers have been grown at 250°C and 600°C. The AFM image in Fig. 3 (a) shows a high nucleation density at 600°C of relatively small and round-shaped nuclei, for which it is not possible to distinguish the mirror twins. We propose an alternative method using X-ray photoelectron diffraction (XPD). It consists in measuring the total intensity of a core level in XPS at different angles. The photoelectrons with kinetic energy greater than 1 keV are expected to be mostly forward scattered by the surrounding atoms.[43,44] Neglecting the back-scattering and assuming a very small proportion of bilayer in 0.3 ML-thick samples, the Ta $4f$ electrons can only be scattered by Se atoms

in the top layer. As illustrated in Fig. 3 (b), the three nearest neighbors of the Ta atoms lie at a polar angle of 37.8° (for 1T) from the layer plane,[45] while they are separated by 120° in the azimuthal plane. Hence, if all grains have the same orientation and phase, three peaks should be recorded in XPD upon a full scan of the azimuthal angle at a fixed polar angle of 37.8°, corresponding to the three directions in which the analyzer is aligned with the Ta-Se bonds. It should be noted that the 1H and 1T phases have the upper plane of Se atoms rotated by 60° if the bottom planes are aligned. Thus, if six peaks separated by 60° are obtained, it could be either caused by mirror twins or a phase mix.

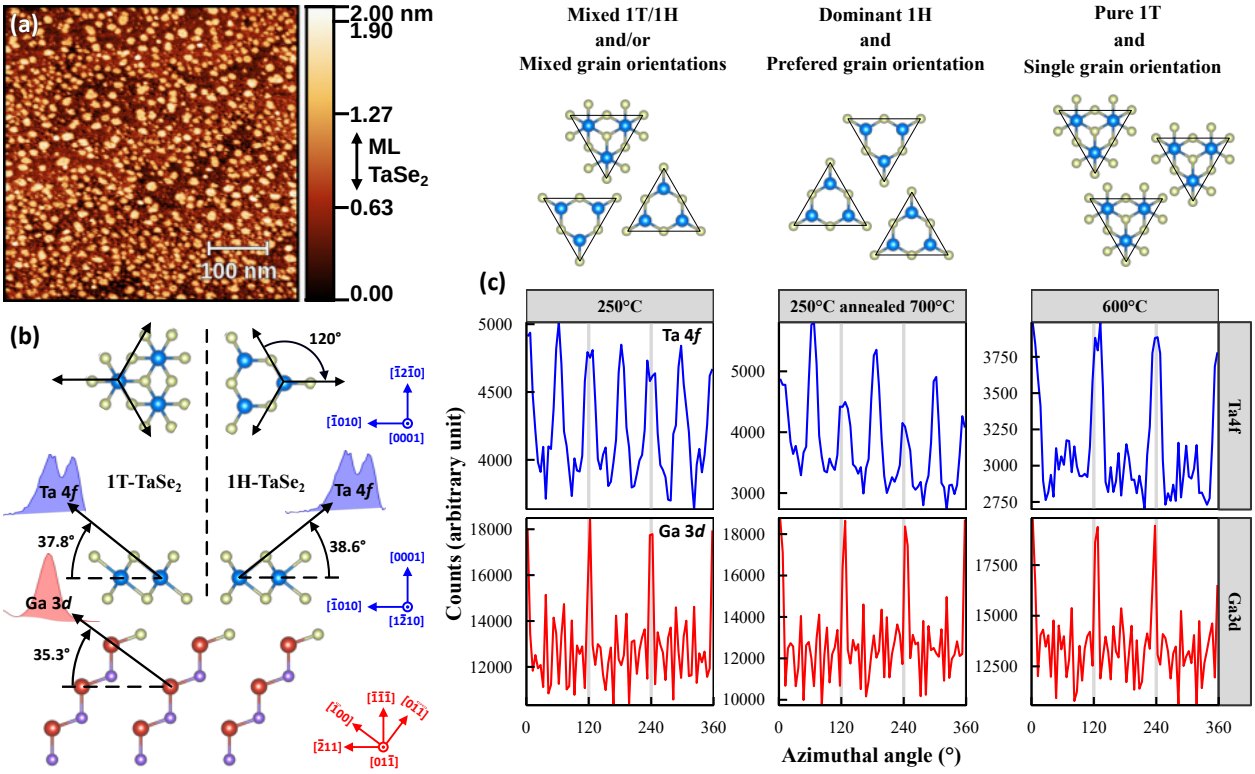

Figure 3: (a) AFM image of a 0.3 ML-thick $TaSe_2$ layer grown at 600°C. (b) Schematics of the photodiffraction angles considered in this experiment. (c) Azimuthal XPD spectra recorded for three samples at constant polar angle of 37.8°C for the Ta 4f and Ga 3d CLs.

The samples were first aligned along a $[\bar{2}\,1\,1]$ direction of the substrate. Then, the Ta 4f and Ga 3d CLs were simultaneously recorded every 2.5° from 0 to 360°. Their peak intensities, measured as the total area after a Shirley background subtraction,[46] are presented in Fig. 3 (c). For all samples, the Ga 3d intensity exhibits three narrow peaks, that are attributed to

an alignment of Ga atoms along the $[\bar{1}\,0\,0]$ direction. Despite the calculated angle is 35.3°, the width of the XPD peak and the 2° half-aperture of the analyzer makes its detection possible at 37.8°. Concerning the Ta $4f$ intensity, six peaks of similar height are found on the as-grown 250°C-sample. After annealing, these six peaks are still visible, but three of them are clearly more intense. It can be related to a better phase purity, as the 1H is known to be predominant in this case, or to a rearrangement towards the most stable grain orientation. On the other hand, when the sample is grown at 600°C, only 3 peaks are obtained in accordance to a good phase purity and unique grain orientation. Note that the Ta $4f$ peaks are aligned with the Ga $3d$ peaks in this latter case, while the main peaks were shifted by 60° in the annealed 250°C sample. This is in good agreement with the inversion symmetry in 1T. It means that, in both cases, the bottom Ta-Se bonds are oriented in the same direction relatively to the Ga-P ones, and only the top Se atoms are placed differently in 1T or 1H. Since grains of different phase or orientation are not expected to coalesce, only a high growth temperature could lead to the formation of a monocrystalline film.

3.3 Growth of $TaSe_2$ multilayers

One of the benefits of MBE is the precise control of the thickness as no catalytic effect from the substrate is expected. Hence 5 ML-thick $TaSe_2$ samples have been grown at 250, 400, 500, 550 and 600°C by increasing the growth duration. Similar to the monolayers, the RHEED patterns of the as-grown samples are either diffuse or spotty as-grown (Fig. 4 (a-e)). Annealing the samples at either 650 or 700°C improves the RHEED pattern. As shown in Fig. 4 (f-j) thin streaks are obtained, although spots remain for the samples grown at 500°C and above. Note that the RHEED patterns of the samples grown at 500 and 550°C seem slightly diffuse after annealing and cooling, possibly due to a very weak superstructure caused by the CDW of the octahedrally coordinated layers.

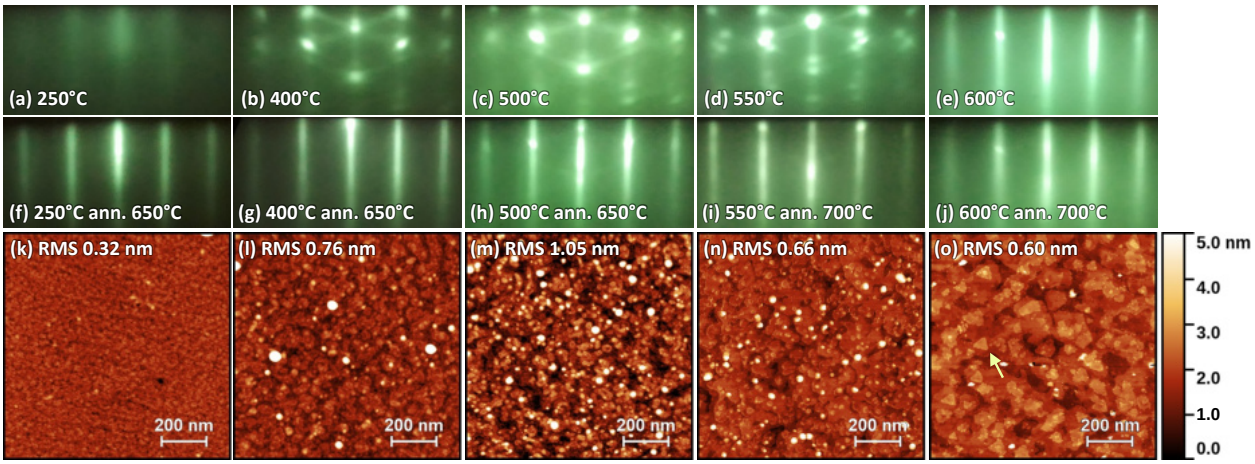

Figure 4: (a-e) RHEED patterns along a $[1\,0\,\bar{1}\,0]$ direction of 5 MLs-thick $TaSe_2$ multilayers grown at 250°C, 400°C, 500°C, 550°C and 600°C. (f-j) RHEED patterns of the same samples after annealing. (k-o) AFM images of the annealed samples. All images share the same color scale. On image (o), a yellow arrow points to a grain with a triangular shape.

AFM images of the corresponding annealed samples are presented Fig. 4 (k-o). An increase of the roughness is clearly observed from 250 to 500°C, confirmed by the root mean square (RMS) of height differences calculated on the whole image. The sample grown at 250°C exhibits a small-scale roughness and a particularly uniform coverage. On the 400° and 500°C-grown samples, wider islands are formed, characterized by an increased number of ML-steps from the islands to the holes. In addition, 5 to 10 nm-high protrusions are observed whose density is maximum for the sample grown at 500°C, in accordance with the presence of spots on the RHEED pattern. When the growth temperature is further increased, the density of protrusions decreases as well as the RMS, and 50-100 nm large terraces are obtained, some of which having triangular shapes at 600°C.

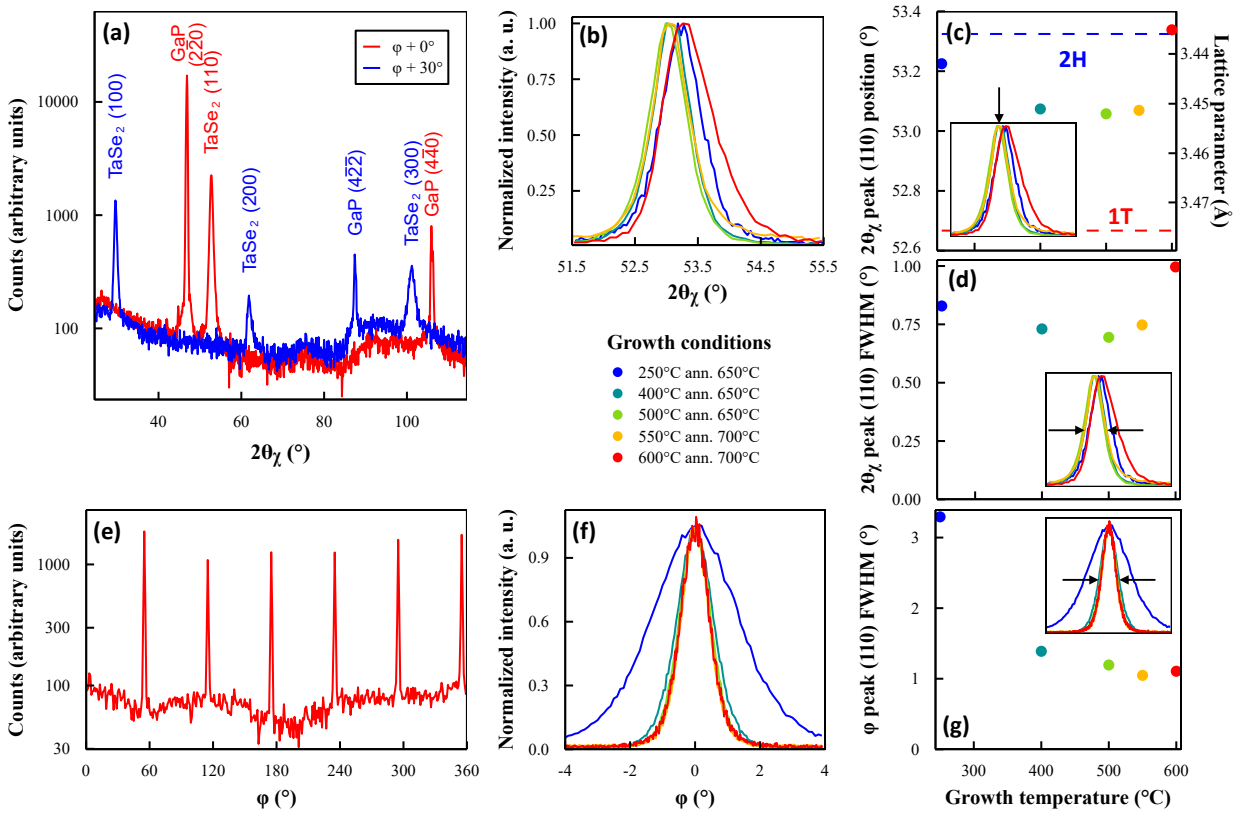

Figure 5: (a) GIXRD radial ($2\theta_\chi$-φ) scans of the 5 ML-thick $TaSe_2$ multilayer grown at 550°C and annealed at 600°C along two different directions of the substrate. (b) Comparison of the (1 1 0) peaks obtained for the 5 samples. (c) Evolution of the $2\theta_\chi$ positions of the (1 1 0) peaks in plot (b), and cell parameters with the growth temperature. Reference for 2H and 1T phase are from ref.[45] (d) Full widths at half maximum (FWHM) of the peaks in plot (b) as a function of growth temperature. (e) Full azimuthal (φ) scan on the (1 1 0) peak of the sample presented in plot (a). (f) Comparison of the peaks obtained by azimuthal scans on the five samples. (g) FWHM of the peaks in plot (f).

To study the influence of the growth temperature on the crystalline quality, in-plane GIXRD measurements were performed using a Rigaku SmartLab X-ray diffractometer at a fixed 0.5° incidence angle. Typical diffraction patterns ($2\theta_\chi$-φ scans) along the $[1\,0\,\bar{1}\,0]$ and $[1\,1\,\bar{2}\,0]$ directions of the layer are presented Fig. 5 (a). The main peaks have been attributed to either the substrate or the layer. The $(2\,\bar{2}\,0)$ and $(4\,\bar{4}\,0)$ peaks of substrate have been used as references for angle calibration and we then focus on the most intense $TaSe_2$ (1 1 0) peak whose intensity has been normalized. Fig. 5 (b) reports its evolution for different

growth and annealing temperatures and evidences a shift with increasing temperatures and a broadening at the highest one. The lattice parameter deduced from the peak position in Fig. 5 (c) is 3.44 ± 0.01 Å for the sample grown at 250°C in good agreement with the lattice parameter of the 2H-phase found in the literature.[47] When the temperature is increased, the peak position is first slightly shifted towards smaller angles (larger lattice constants), and then towards larger angles (smaller lattice constants) for growth temperatures above 500°C. Simultaneously, the peak becomes asymmetric, indicating a minority phase or a lattice parameter gradient. Likewise, the full width at half maximum (FWHM) of this peak, plotted in Fig. 5 (d), decreases from 0.86° at 250°C to 0.69° at 500°C, in line with an improvement of the grain size with increasing growth temperature, until it raises up to 1.0° at 600 °C. Given the 50-100 nm-large triangular domains observed in AFM at 600°C, the peak width seems no longer limited by the grain size at the highest growth temperatures, but rather by the inhomogeneity of the layers.

For each sample, the azimuthal φ scan reveals only 6 peaks, as seen in Fig. 5 (e), confirming the layer still respects a similar epitaxial relationship with the substrate to that determined for the monolayers in the first section. To study the residual in-plane misorientation, the (110) peaks recorded on all the samples are compared in Fig. 5 (f) and the corresponding FWHM are plotted in Fig. 5 (g). The decrease of the FWHM from 250°C to 400°C indicates a better alignment between both lattices, which further improves at higher temperatures, albeit to a lesser extent.

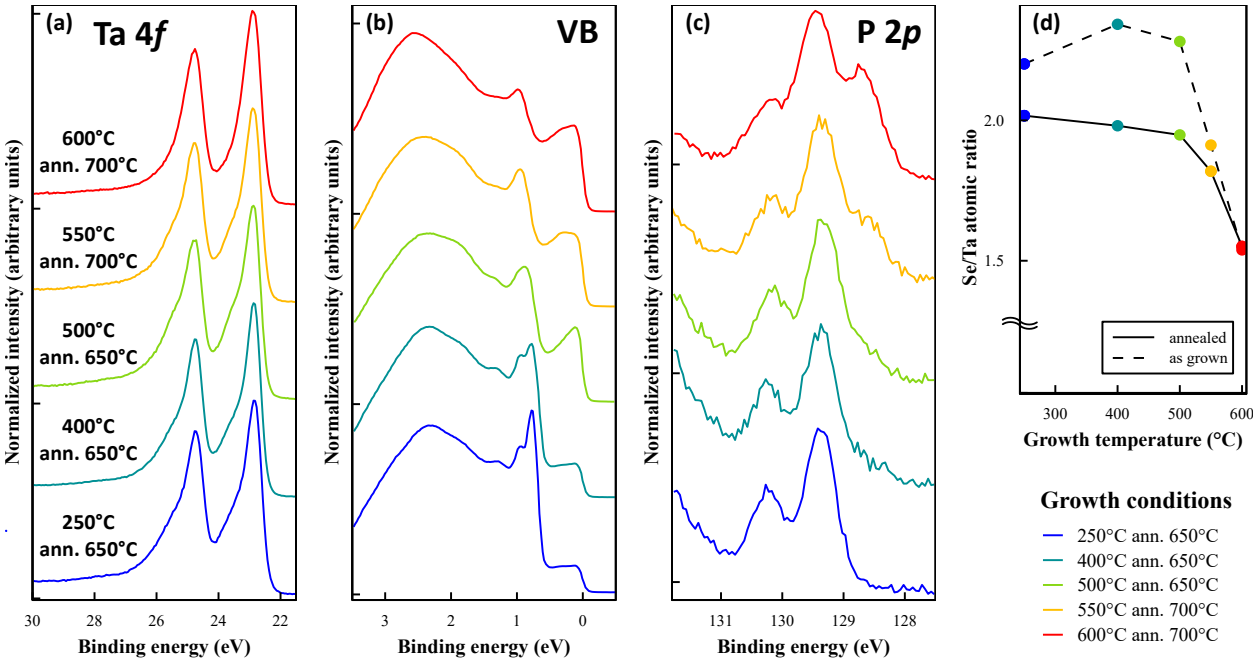

Figure 6: (a) Ta $4f$ CLs measured in XPS at an emission angle of 45°. (b) Valence band measured in UPS around Γ. (c) P $2p$ CLs at 45°. (d) Atomic composition of the layers deduced from XPS measurements at an emission angle of 25° so that signal originating from Se-terminated GaP substrate is negligible.

To determine if the asymmetry and shift measured in GIXRD are caused by a phase change, the samples have been further analyzed by XPS and UPS. The Ta $4f$ CLs and valence band are plotted in Fig. 6 (a) and (b) respectively. The sample grown at 250°C and annealed at 650°C exhibits a similar spectrum to the monolayer prepared in the same conditions and attributed to the 1H phase. The shape of the valence band is comparable to that of Fig. 2 but exhibits an additional narrow peak at 0.8 eV. As for the samples grown at higher temperatures, neither the CDW splitting of the Ta $4f$ CLs, nor the peaks in the valence band attributed to the 1T phase appear clearly. Instead, both the characteristic shoulder of 2H-$TaSe_2$ in the Ta $4f$ CLs and the narrow peaks at 0.8 and 1 eV fade, which might indicate that the $TaSe_2$ layer becomes more defective or converted into a mixture of different phases. To answer this question, a quantitative analysis was derived from the Se $3d$ over Ta $4f$ CL intensity ratios corrected for the relative sensitivity factors[31] in the as-grown and annealed layers (Fig. 6 (d)). Before annealing, all layers grown at 500°C or

below have a Se/Ta ratio slightly above the expected stoichiometry while the samples grown at 550 and 600°C are clearly below. After annealing, the Se/Ta ratio decreased for most samples and especially all layers that were Se-rich have now a ratio near or slightly below 2. On the contrary, the ratio remains stable for the sample grown at 600°C, even though it was already highly Se-deficient. Besides, the increase of the annealing temperature from 650°C to 700°C is not found to have a significant influence on the stoichiometry (Supplementary 4). Finally, the annealing may remove excess Se but does not seem to degrade the samples up to 700°C. By contrast, a high growth temperature seems to deteriorate the material due to Se-deficiency, especially at 550°C and above.

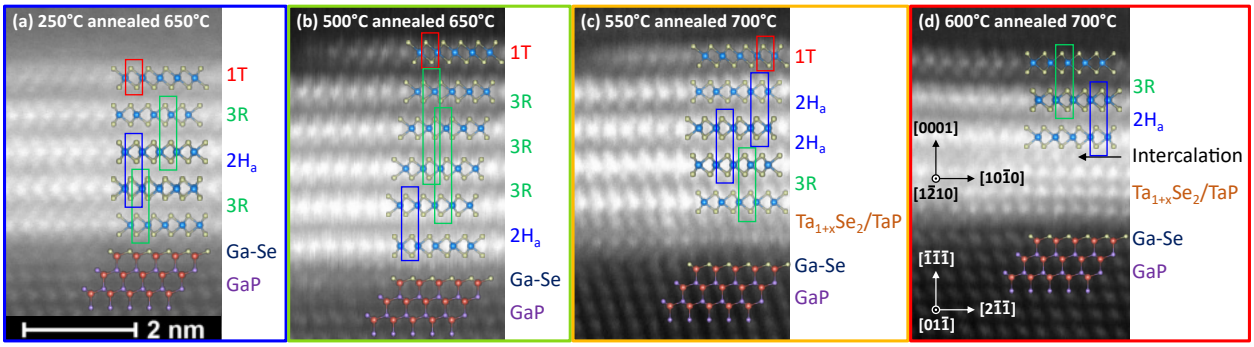

Figure 7: STEM images of the samples grown at 250°C and annealed at 650°C (a), 500°C and annealed at 650°C (b), 550°C and annealed at 700°C (c), 600°C and annealed at 700°C (d).

For a deeper analysis of the resulting compound, cross-sectional STEM lamellae have been prepared along the $[1\,\bar{1}\,0]$ GaP zone axis and are presented Fig. 7. Regardless of the growth temperature, only a small amount of 1T phase is detected, which only resides at the top of the stacking where its in-plane extent is limited. In an early study, it has been proposed that metastable octahedrally coordinated (1T-like) layers are formed because molecules are generally stable with octahedral coordination and could be preserved at low temperature by quenching.[23] An XPS analysis of the as-grown layers (Supplementary 5) reveals that a small amount of 1T-$TaSe_2$ may indeed be formed even if the samples predominantly consist of the 2H phase. The observation that some 1T survives at the top of the layer even after annealing suggests that it is more stable at this position, consistent with the stability of

the 1T phase in monolayer discussed in the first section. These results further support the idea that dimensionality affects the phase stability and explains why under similar growth conditions, the 1T phase can be grown in monolayer and not in multilayers.

The samples grown at 250 and 500°C exhibits mostly trigonal prismatic (1H) layers stacked in the same orientation, which corresponds to the 3R stacking. However, this stacking is kept for only few monolayers until the layer orientation is flipped which corresponds locally to a $2H_a$ stacking. Such stacking faults are directly related to the formation of mirror twins and appears as one of the fundamental limitations of MBE for growing low-defect TMDCs.[48] For a growth temperature of 600°C, and to a lesser extent 550°C, a denser structure without vdW gap is clearly distinguishable at the interface with the substrate whereas pristine 1H layers are observed at the top of the stacking. Between these two regions, we can notice intercalated Ta atoms within 1H layers. It is in agreement with the excess of Ta measured in these layers by XPS. However, the close-packed phase remains to be identified. A fit of the Ta $4f$ does not reveal any additional peak (Supplementary 6), as it would be expected if metallic Ta was formed. Instead, it could be attributed to 2H-$Ta_{1+x}Se_2$ with a full occupation of the intercalation sites. An increase of the lattice parameter of bulk crystals was reported in the range $0.03 < x < 0.25$, followed by a decrease for $0.25 < x < 0.64$.[45] This is in good agreement with our measurement of a larger lattice parameter for the slightly Ta-rich 2H-$TaSe_2$ phase grown between 400°C and 550°C, and a smaller lattice parameter for the most Se-deficient sample grown at 600°C. Besides, the P $2p$ CLs (Fig. 6 (c)) exhibit a new component at low binding energies for samples grown at 550°C and above, suggesting the formation of Ta-P bonds, given the smaller electronegativity of Ta compared to Ga. Hence, the closed-packed phase may also be related to an intermediate TaP layer. This compound normally crystallizes into a tetragonal lattice, but was also reported to form a metastable tungsten carbide-like structure,[49,50] which is hexagonal and belongs to the same space group as $2H_b$-$Ta_{1+x}Se_2$.[6] Such a structure would favor a miscibility of the two compounds. We note that unlike the Se-deficiency, the Ta-P component is not present in the as-grown samples

(Supplementary 7). It is then possible that the phosphorus atoms from the substrate react with the excess Ta atoms in the already Se-deficient layers during the annealing, which explains why Ta-P bonds appear only in the samples grown at high temperatures.

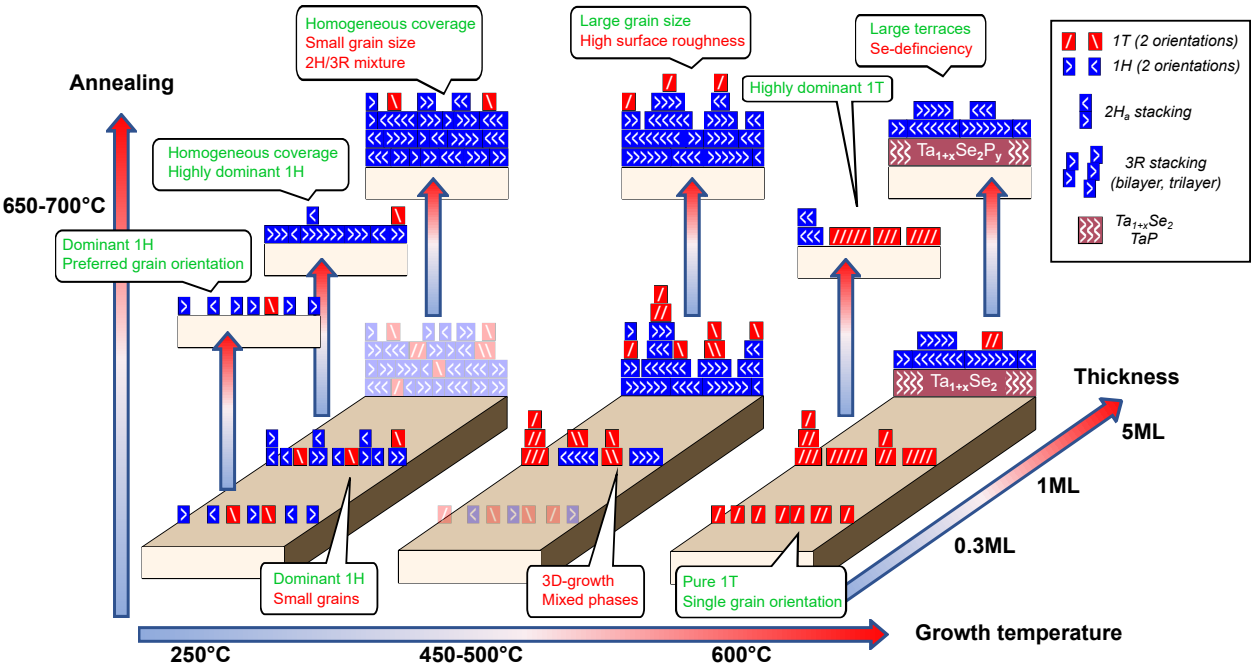

Figure 8: Phase and growth diagram of $TaSe_2$ on GaP. The configurations that were insufficiently characterized are represented with semi-transparency.

Figure 8 gathers the results of the growth of $TaSe_2$ presented in this paper. It highlights the influence of the thickness on the phase formation, especially for the layers grown at high temperatures. It suggests that the 1T-phase converts to 1H layers as soon as more than one monolayer is grown. Then, as the growth continues, the layers closer to the substrate start to become Se-deficient which contributes to its reaction with the substrate after annealing. It may occur because the formation of new $TaSe_2$ layers on top of the staking reduces the Se supply. This mechanism explains how a pristine $TaSe_2$ can be maintained on top of the stacking at temperature as high as 600°C, while the bottom layers already degrade at 550°C. It highlights that the growth of $TaSe_2$ multilayers is significantly more challenging than monolayers. In particular, the formation of multilayer 1T-$TaSe_2$ by MBE is unlikely as this phase requires a temperature above 780°C to be stable in bulk.[40] A satisfying stoichiometry

was demonstrated up to 500°C but the vdW nature of the $TaSe_2$/GaP-Se interface remains less obvious than in a WSe_2/GaP-Se heterostructure prepared under similar conditions.[51] This observation suggests a particular affinity between Ta and P atoms, calling for less reactive substrates for vdW $TaSe_2$ multilayers fabrication.

3.4 Electrical characterization

Still, one of the advantages of using GaP substrates is the availability of both doped and semi-insulating wafers. Hence, $TaSe_2$ multilayers have also been grown at 250°C, 400°C and 500°C on semi-insulating GaP and protected with a thin Se capping layer for electrical transport characterization. The sheet resistance is measured with the four-point probes method using tungsten probes directly placed on the layer (Fig. 9 (a)). A resistivity of $(1.8 \pm 0.7) \times 10^{-4}$ Ω.cm is obtained at room temperature for the sample grown at 250°C and annealed at 650°C (Supplementary 8), in relatively good agreement with the literature for bulk 2H-$TaSe_2$.[7,52,53] Besides, the temperature dependence was measured under vacuum in a cryogenic setup as seen in Fig. 9 (b). The linear increase of the resistivity with temperature indicates a metallic behavior, though no resistance drop related to a CDW transition is measured around 122K. It is in contrast to what was reported for 2H-$TaSe_2$[7,52] and better agrees with the weakening of the CDW reported in 3R-$TaSe_2$.[12,16]

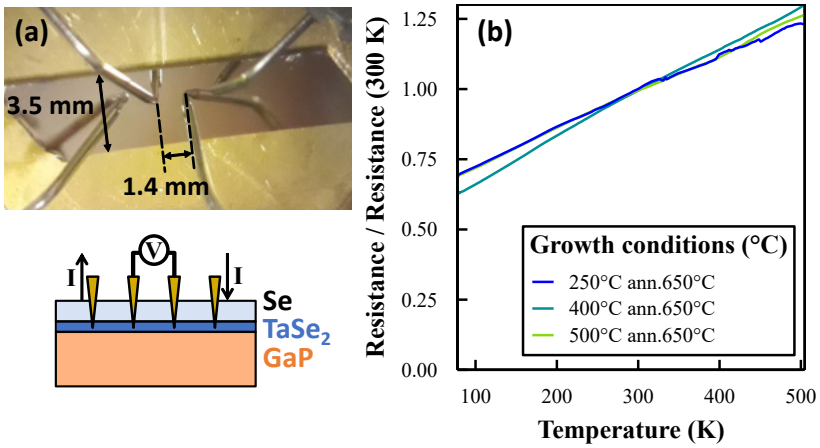

Figure 9: (a) Picture and schematics of the four-point probe measurement. (b) Temperature dependence of the resistance for 3 samples grown at different temperatures.

For every sample, a high work function 5.5±0.1 eV (Supplementary 9) is deduced from the secondary electron cutoff in UPS in perfect agreement with the literature.[24] It makes $TaSe_2$ a good candidate for high work function metallic contact. Because, the oxidation of $TaSe_2$ in air may be an issue,[54] electrical measurements have been performed after evaporation of the Se capping layer to estimate the oxidation rate. The conductivity decreases with time but remains more than 60 % of its initial value after 3 days. The partial oxidation of $TaSe_2$ is clearly shown by angle-dependent XPS measurements (Supplementary 10). Both Ta-O and Ta-Se bonds are seen, with the Ta-O peaks being more pronounced at small take-off angles. Hence the oxidation is mostly located close to the surface, in agreement with a layer-by-layer oxidation. No self-passivation was measured at this stage but it has been reported for thicker $TaSe_2$ crystals,[55] highlighting the importance of growing thick $TaSe_2$ layers for more stable contacts.

4 Conclusion

This study establishes GaP as a promising substrate for vdW epitaxy of both metallic 1H and Mott-insulating 1T-$TaSe_2$ monolayers. Especially, it enables the growth of highly oriented 1T-$TaSe_2$ without mirror twin boundaries at high growth temperature. By contrast, significantly lower temperatures must be used for multilayer growth to avoid the loss of Se atoms and the formation of an undesired compound at the GaP-$TaSe_2$ interface. STEM images reveal a mixture of $2H_a$ and 3R polytypes in multilayer along with the occurrence of the 1T phase located at the top of the stacking. This is attributed to the higher stability of the 2H phase in bulk which converts the 1T phase into 2H phase as soon as a monolayer is completed. These results give a better understanding of the effects of growth temperature, annealing and thickness of MBE-grown $TaSe_2$. Notably, as a general trend, a high growth temperature improved the crystalline quality at the cost of a degraded morphology, whereas an annealing is beneficial for both. Finally, an electrical characterization pinpoints $TaSe_2$

multilayers as potential metallic contacts for 2D-material based devices.

Acknowledgement

We acknowledge the financial support from the Tunne2D (ANR-21-CE24-0030), ADICT (ANR-22-PEEL-0011) and NANODYN (ANR-21-CE24-0001-01) projects, as well as from the French technological network RENATECH and Region Hauts-de-France for funding CMNF and PCP platforms. Chevreul Institute (CNRS FR2638) is acknowledged for funding X-ray facilities.

Supporting Information Available

The following files are available free of charge.

- Supporting information: Additional AFM, XPS and UPS characterizations of the samples, experimental details for the resistivity calculation, work function measurement and Ta $4f$ CLs of an oxidized layer (PDF)

References

(1) Wang, Q. H.; Kalantar-Zadeh, K.; Kis, A.; Coleman, J. N.; Strano, M. S. Electronics and optoelectronics of two-dimensional transition metal dichalcogenides. *Nature nanotechnology* **2012**, *7*, 699–712.

(2) Bark, H.; Choi, Y.; Jung, J.; Kim, J. H.; Kwon, H.; Lee, J.; Lee, Z.; Cho, J. H.; Lee, C.

Large-area niobium disulfide thin films as transparent electrodes for devices based on two-dimensional materials. *Nanoscale* **2018**, *10*, 1056–1062.

(3) Shi, J.; Huan, Y.; Zhao, X.; Yang, P.; Hong, M.; Xie, C.; Pennycook, S.; Zhang, Y. Two-dimensional metallic vanadium ditelluride as a high-performance electrode material. *ACS nano* **2021**, *15*, 1858–1868.

(4) Qiao, P.; Xia, J.; Li, X.-Z.; Li, Y.; Cao, J.; Zhang, Z.; Lu, H.; Meng, Q.; Li, J.; Meng, X. Epitaxial van der Waals contacts of 2D $TaSe_2$-WSe_2 metal-semiconductor heterostructures. *Nanoscale* **2023**, *15*, 17036–17044.

(5) Lasek, K.; Li, J.; Kolekar, S.; Coelho, P. M.; Zhang, M.; Wang, Z.; Batzill, M., et al. Synthesis and characterization of 2D transition metal dichalcogenides: Recent progress from a vacuum surface science perspective. *Surface Science Reports* **2021**, *76*, 100523.

(6) Katzke, H.; Tolédano, P.; Depmeier, W. Phase transitions between polytypes and intralayer superstructures in transition metal dichalcogenides. *Physical Review B* **2004**, *69*, 134111.

(7) Di Salvo, F. J.; Moncton, D. E.; Wilson, J. A.; Mahajan, S. Coexistence of two charge-density waves of different symmetry in $4Hb-TaSe_2$. *Phys. Rev. B* **1976**, *14*, 1543–1546.

(8) Nakata, Y.; Sugawara, K.; Chainani, A.; Oka, H.; Bao, C.; Zhou, S.; Chuang, P.-Y.; Cheng, C.-M.; Kawakami, T.; Saruta, Y., et al. Robust charge-density wave strengthened by electron correlations in monolayer 1T-$TaSe_2$ and 1T-$NbSe_2$. *Nature communications* **2021**, *12*, 5873.

(9) Yoshida, M.; Suzuki, R.; Zhang, Y.; Nakano, M.; Iwasa, Y. Memristive phase switching in two-dimensional 1T-TaS_2 crystals. *Science advances* **2015**, *1*, e1500606.

(10) Moncton, D. E.; Axe, J. D.; DiSalvo, F. J. Study of superlattice formation in 2H-$NbSe_2$ and 2H-$TaSe_2$ by neutron scattering. *Physical Review Letters* **1975**, *34*, 734.

(11) Van Maaren, M. H.; Schaeffer, G. M. Some new superconducting group Va dichalcogenides. *Physics Letters A* **1967**, *24*, 645–646.

(12) Deng, Y.; Lai, Y.; Zhao, X.; Wang, X.; Zhu, C.; Huang, K.; Zhu, C.; Zhou, J.; Zeng, Q.; Duan, R., et al. Controlled Growth of 3R Phase Tantalum Diselenide and Its Enhanced Superconductivity. *Journal of the American Chemical Society* **2020**, *142*, 2948–2955.

(13) Xing, Y.; Yang, P.; Ge, J.; Yan, J.; Luo, J.; Ji, H.; Yang, Z.; Li, Y.; Wang, Z.; Liu, Y., et al. Extrinsic and intrinsic anomalous metallic states in transition metal dichalcogenide Ising superconductors. *Nano Letters* **2021**, *21*, 7486–7494.

(14) Bhoi, D.; Khim, S.; Nam, W.; Lee, B. S.; Kim, C.; Jeon, B.-G.; Min, B. H.; Park, S.; Kim, K. H. Interplay of charge density wave and multiband superconductivity in 2H-$Pd_x TaSe_2$. *Scientific reports* **2016**, *6*, 24068.

(15) Li, L.; Deng, X.; Wang, Z.; Liu, Y.; Abeykoon, M.; Dooryhee, E.; Tomic, A.; Huang, Y.; Warren, J. B.; Bozin, E. S., et al. Superconducting order from disorder in 2H-$TaSe_{2-x}S_x$. *npj Quantum Materials* **2017**, *2*, 11.

(16) Tanaka, Y.; Matsuoka, H.; Nakano, M.; Wang, Y.; Sasakura, S.; Kobayashi, K.; Iwasa, Y. Superconducting 3R-$Ta_{1+x}Se_2$ with Giant In-Plane Upper Critical Fields. *Nano Letters* **2020**, *20*, 1725–1730.

(17) Li, X. C.; Zhou, M. H.; Dong, C. Superconductivity enhancement in $Ta_{1+x}Se_2$ with a randomly stacked structure. *Superconductor Science and Technology* **2019**, *32*, 035001.

(18) Luo, H.; Xie, W.; Seibel, E. M.; Cava, R. J. Superconductivity in 3R-Ta1- xMxSe2 (M= W, Mo). *Journal of Physics: Condensed Matter* **2015**, *27*, 365701.

(19) Bai, H.; Wang, M.; Yang, X.; Li, Y.; Ma, J.; Sun, X.; Tao, Q.; Li, L.; Xu, Z.-A. Superconductivity in tantalum self-intercalated 4Ha-Ta1. 03Se2. *Journal of Physics: Condensed Matter* **2018**, *30*, 095703.

(20) Baek, S.-H.; Sur, Y.; Kim, K. H.; Vojta, M.; Büchner, B. Interplay of charge density waves, disorder, and superconductivity in 2H-$TaSe_2$ elucidated by NMR. *New Journal of Physics* **2022**, *24*, 043008.

(21) Shi, J.; Chen, X.; Zhao, L.; Gong, Y.; Hong, M.; Huan, Y.; Zhang, Z.; Yang, P.; Li, Y.; Zhang, Q., et al. Chemical Vapor Deposition Grown Wafer-Scale 2D Tantalum Diselenide with Robust Charge-Density-Wave Order. *Advanced Materials* **2018**, *30*, 1804616.

(22) Shimada, T.; Ohuchi, F. S.; Parkinson, B. A. Epitaxial growth and charge density wave of $TaSe_2$. *MRS Online Proceedings Library (OPL)* **1991**, *230*, 231–236.

(23) Shimada, T.; Nishikawa, H.; Koma, A.; Furukawa, Y.; Arakawa, E.; Takeshita, K.; Matsushita, T.-i. Polytypes and crystallinity of ultrathin epitaxial films of layered materials studied with grazing incidence X-ray diffraction. *Surface science* **1996**, *369*, 379–384.

(24) Tsoutsou, D.; Aretouli, K. E.; Tsipas, P.; Marquez-Velasco, J.; Xenogiannopoulou, E.; Kelaidis, N.; Aminalragia Giamini, S.; Dimoulas, A. Epitaxial 2D $MoSe_2$ ($HfSe_2$) semiconductor/2D $TaSe_2$ metal van der Waals heterostructures. *ACS applied materials & interfaces* **2016**, *8*, 1836–1841.

(25) Nakata, Y.; Yoshizawa, T.; Sugawara, K.; Umemoto, Y.; Takahashi, T.; Sato, T. Selective fabrication of Mott-insulating and metallic monolayer $TaSe_2$. *ACS Applied Nano Materials* **2018**, *1*, 1456–1460.

(26) Lee, H.; Im, H.; Choi, B. K.; Park, K.; Chen, Y.; Ruan, W.; Zhong, Y.; Lee, J.-E.; Ryu, H.; Crommie, M. F., et al. Controlling structure and interfacial interaction of monolayer TaSe2 on bilayer graphene. *Nano Convergence* **2024**, *11*, 1–8.

(27) Ohtake, A.; Goto, S.; Nakamura, J. Atomic structure and passivated nature of the Se-treated GaAs (111) B surface. *Scientific Reports* **2018**, *8*, 1220.

(28) Baillargeon, J. N.; Cheng, K. Y.; Hsieh, K. C. Surface structure of (100) GaP grown by gas source molecular beam epitaxy. *Applied physics letters* **1990**, *56*, 2201–2203.

(29) Foxon, C. T.; Harvey, J. A.; Joyce, B. A. The evaporation of GaAs under equilibrium and non-equilibrium conditions using a modulated beam technique. *Journal of Physics and Chemistry of Solids* **1973**, *34*, 1693–1701.

(30) Koussir, H.; Chernukha, Y.; Sthioul, C.; Haber, E.; Peric, N.; Biadala, L.; Capiod, P.; Berthe, M.; Lefebvre, I.; Wallart, X., et al. Large-area epitaxial Mott insulating 1T-$TaSe_2$ monolayer on GaP(111)B. *Nano Letters* **2023**, *23*, 9413–9419.

(31) Scofield, J. H. Hartree-Slater subshell photoionization cross-sections at 1254 and 1487 eV. *Journal of Electron Spectroscopy and Related Phenomena* **1976**, *8*, 129–137.

(32) Yeh, J. J.; Lindau, I. Atomic subshell photoionization cross sections and asymmetry parameters: $1 \leq Z \leq 103$. *Atomic data and nuclear data tables* **1985**, *32*, 1–155.

(33) Powell, C. J.; Jablonski, A. *NIST Electron Effective-Attenuation-Length Database*; 2011.

(34) Jablonski, A. Evaluation of procedures for overlayer thickness determination from XPS intensities. *Surface Science* **2019**, *688*, 14–24.

(35) Nečas, D.; Klapetek, P. Gwyddion: an open-source software for SPM data analysis. *Open Physics* **2012**, *10*, 181–188.

(36) Horiba, K.; Ono, K.; Oh, J. H.; Kihara, T.; Nakazono, S.; Oshima, M.; Shiino, O.; Yeom, H. W.; Kakizaki, A.; Aiura, Y. Charge-density wave and three-dimensional Fermi surface in 1T-$TaSe_2$ studied by photoemission spectroscopy. *Physical Review B* **2002**, *66*, 073106.

(37) Yan, J.-A.; Cruz, M. A. D.; Cook, B.; Varga, K. Structural, electronic and vibrational properties of few-layer 2H-and 1T-$TaSe_2$. *Scientific reports* **2015**, *5*, 1–13.

(38) Adachi, S. *Physical properties of III-V semiconductor compounds*; John Wiley & Sons, 1992.

(39) Brauer, H. E.; Starnberg, H. I.; Holleboom, L. J.; Hughes, H. P.; Strocov, V. N. Na and Cs intercalation of 2H-$TaSe_2$ studied by photoemission. *Journal of Physics: Condensed Matter* **2001**, *13*, 9879.

(40) Huisman, R.; Jellinek, F. On the polymorphism of tantalum diselenide. *Journal of the Less Common Metals* **1969**, *17*, 111–117.

(41) Latychevskaia, T.; Zan, R.; Morozov, S.; Novoselov, K. S. Symmetry of diffraction patterns of two-dimensional crystal structures. *Ultramicroscopy* **2021**, *228*, 113336.

(42) Mortelmans, W.; De Smet, K.; Meng, R.; Houssa, M.; De Gendt, S.; Heyns, M.; Merckling, C. Role of Stronger Interlayer van der Waals Coupling in Twin-Free Molecular Beam Epitaxy of 2D Chalcogenides. *Advanced Materials Interfaces* **2021**, *8*, 2100438.

(43) Fadley, C. S. Diffraction and holography with photoelectrons and Auger electrons: some new directions. *Surface science reports* **1993**, *19*, 231–264.

(44) de Lima, L. H.; de Siervo, A. X-ray photoelectron diffraction as a modern tool for determining surface stacking sequence in layered materials. *2D Materials* **2024**, *11*, 025018.

(45) Bjerkelund, E.; Kjkshus, A. On the structural properties of the $Ta_{1+x}Se_2$ phase. *Acta Chem Scand* **1967**, *21*, 513–526.

(46) Shirley, D. A. High-resolution X-ray photoemission spectrum of the valence bands of gold. *Physical Review B* **1972**, *5*, 4709.

(47) Kadijk, F.; Huisman, R.; Jellinek, F. Niobium and tantalum diselenides. *Recueil des Travaux Chimiques des Pays-Bas* **1964**, *83*, 768–775.

(48) Mortelmans, W.; Mehta, A. N.; Balaji, Y.; El Kazzi, S.; Sergeant, S.; Houssa, M.; De Gendt, S.; Heyns, M.; Merckling, C. Fundamental limitation of van der Waals homoepitaxy by stacking fault formation in WSe_2. *2D Materials* **2020**, *7*, 025027.

(49) Willerström, J.-O. Stacking disorder in NbP, TaP, NbAs and TaAs. *Journal of the Less Common Metals* **1984**, *99*, 273–283.

(50) Besara, T.; Rhodes, D. A.; Chen, K.-W.; Zhang, Q.; Zheng, B.; Xin, Y.; Balicas, L.; Baumbach, R. E.; Siegrist, T. Non-stoichiometry and Defects in the Weyl Semimetals TaAs, TaP, NbAs, and NbP. *Bulletin of the American Physical Society* **2016**, *61*.

(51) Chapuis, N.; Mahmoudi, A.; Coinon, C.; Troadec, D.; Vignaud, D.; Patriarche, G.; Roussel, P.; Ouerghi, A.; Oehler, F.; Wallart, X. Van der Waals epitaxial growth of few layers WSe_2 on $GaP(111)_B$. *2D Materials* **2024**, *11*, 035031.

(52) Vescoli, V.; Degiorgi, L.; Berger, H.; Forró, L. Dynamics of Correlated Two-Dimensional Materials: The 2H-$TaSe_2$ Case. *Physical review letters* **1998**, *81*, 453.

(53) Neal, A. T.; Du, Y.; Liu, H.; Ye, P. D. Two-dimensional $TaSe_2$ metallic crystals: spin–orbit scattering length and breakdown current density. *ACS Nano* **2014**, *8*, 9137–9142.

(54) Li, H.; Lu, G.; Wang, Y.; Yin, Z.; Cong, C.; He, Q.; Wang, L.; Ding, F.; Yu, T.; Zhang, H. Mechanical exfoliation and characterization of single-and few-layer nanosheets of WSe_2, TaS_2, and $TaSe_2$. *small* **2013**, *9*, 1974–1981.

(55) Wang, X.; Tong, L.; Fan, W.; Yan, W.; Su, C.; Wang, D.; Wang, Q.; Yan, H.; Yin, S. Air-stable self-powered photodetector based on $TaSe_2/WS_2/TaSe_2$ asymmetric heterojunction with surface self-passivation. *Journal of Colloid and Interface Science* **2024**, *657*, 529–537.

TOC Graphic

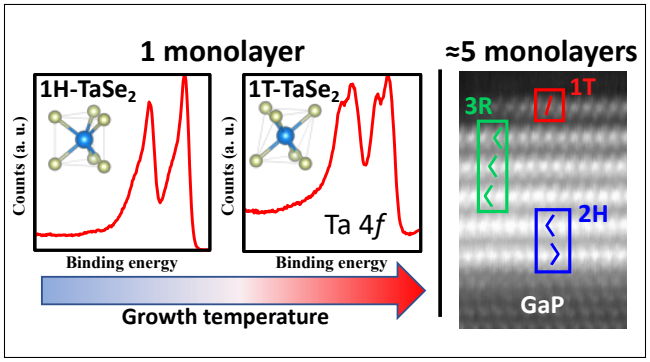
1 monolayer
≈5 monolayers
1H-TaSe2
1T-TaSe2
Counts (a. u.)
Counts (a. u.)
Ta 4f
Binding energy
Binding energy
Growth temperature
3R
1T
2H
GaP

Supporting information

Thickness dependence in phase formation and properties of $TaSe_2$ layers grown on $GaP(111)_B$

Corentin Sthioul*,[1], Yevheniia Chernukha[1], Houda Koussir[1], Christophe Coinon[1], Gilles Patriarche[2], David Troadec[1], Louis Thomas[1], Pascal Roussel[3], Bruno Grandidier[1], Pascale Diener[1] and Xavier Wallart[1]

[1]Univ. Lille, CNRS, Centrale Lille, Univ. Polytechnique Hauts-de-France, Junia-ISEN, UMR 8520 - IEMN, F-59000 Lille, France

[2]Univ. Paris-Saclay, CNRS, Centre de Nanosciences et de Nanotechnologies, 91120 Palaiseau, Paris, France

[3]Unité de Catalyse et de Chimie du Solide (UCCS), Univ. Lille, CNRS, Centrale Lille, Univ. d'Artois, UMR 8181 - UCCS, F-59000 Lille, France

*Corresponding author e-mail : corentin.sthioul@univ-lille.fr

Supplementary 1 AFM 1ML $TaSe_2$ 250°C as-grown

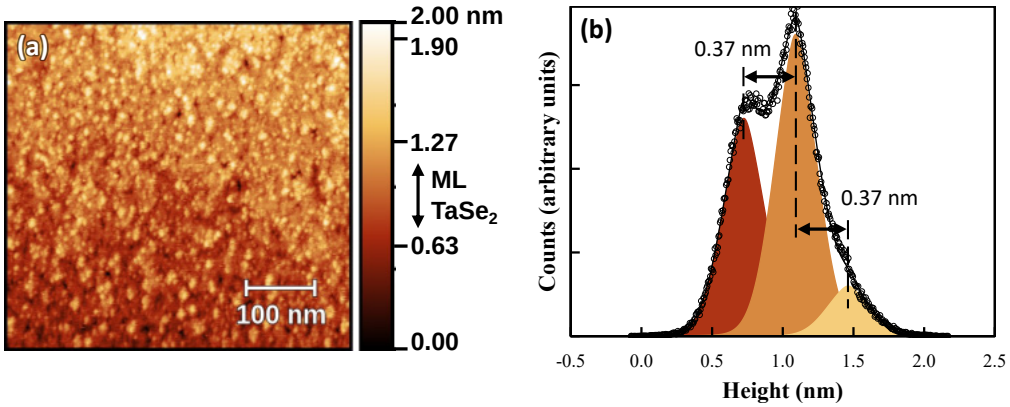

Figure S1: (a) AFM image of a $TaSe_2$ monolayer grown at 250°C before annealing. (b) Histogram of the measured heights from the AFM image, fitted using pseudo-Voigt functions

The AFM image Fig. S1 (a) reveals a morphology with small grains. The atomic steps of the substrate are barely visible on the image and can be evidenced in the histogram of measured height presented in Fig. S1 (b).

Supplementary 2 Ta $4f$ CL decomposition for 1ML 1T-$TaSe_2$

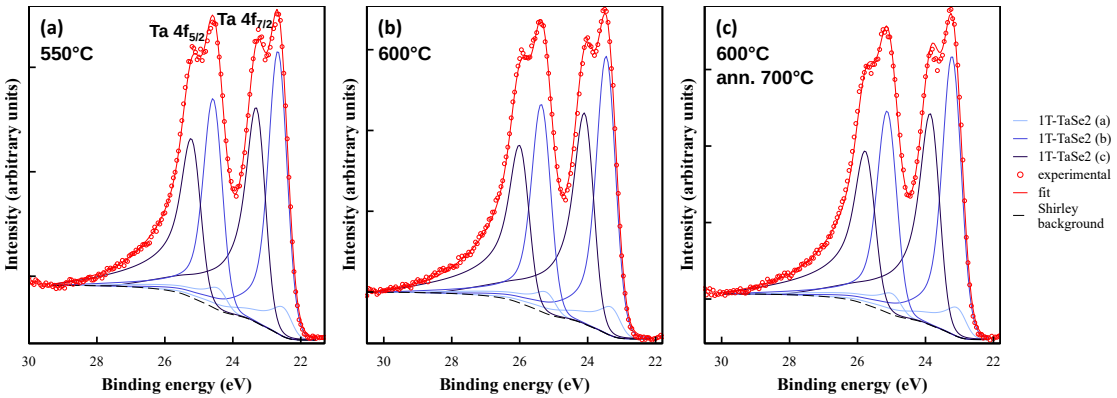

Figure S2: Ta $4f$ CL decomposition for 1T-$TaSe_2$ MLs grown at (a) 550°C, (b) 600°C and (c) 600°C and annealed at 700°C.

The Ta 4_f CL decompositions presented in Fig. S2 reveal three components for the 1T-phase corresponding to the three nonequivalent sites in the CDW (denoted a, b and c) with a 1:6:6 integrated intensity ratio. They are fitted using Doniach-Sunjic-Shirley[1] line shapes, a Doniach-Sunjic-based[2] line shape with finite area. The relative position of the unresolved site a is fixed at -0.23 eV from site b,[3] while the energy shift between site b and c is found to be Δ_{CDW}=0.59 eV in relatively good agreement with the literature.

A good fit is obtained for these three samples by only adjusting the heights, widths and position with respect to E_F, demonstrating that they are all correctly described with 1T-phase only. By contrast, no satisfactory fit could be obtained on the other ML samples. This is attributed to the presence of the 1H phase which is known to exhibit an unusual shoulder[4] that cannot be described by standard line shapes.

Supplementary 3 STM 1ML $TaSe_2$ 600°C annealed 700°C

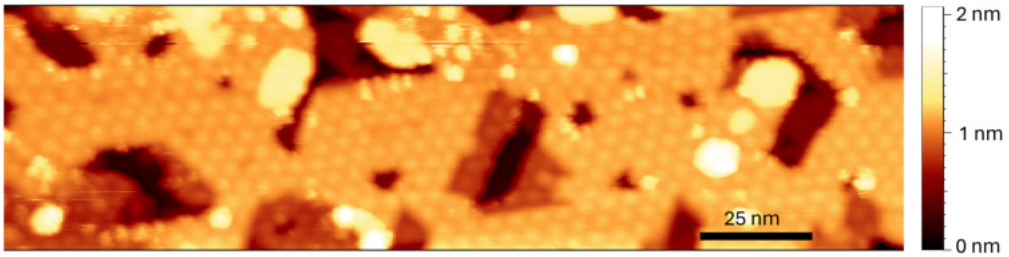

Figure S3: STM image of a $TaSe_2$ monolayer grown at 600°C and annealed at 700°C. Feedback parameters: sample voltage $V_s = 2.0$ V; tunneling current $I_t = 20$ pA; temperature: 77 K.

The STM image in Fig. S3 reveals more in detail the morphology of the sample grown at 600°C after annealing. The crystalline coherence of the domains is confirmed by the presence of a continuous moiré, although locally distorted around point defects.

Supplementary 4 Influence of the annealing temperature

Annealing temperatures of 650 and 700°C have been used in this study. Because the growth temperature is shown to have a significant impact on the layer, especially at high temperature where a significant degradation is found at 600°C, the annealing temperature also might have an influence. To elucidate this question, 5ML-thick $TaSe_2$ layers grown at 250°C and annealed at either 650 or 700°C, are compared.

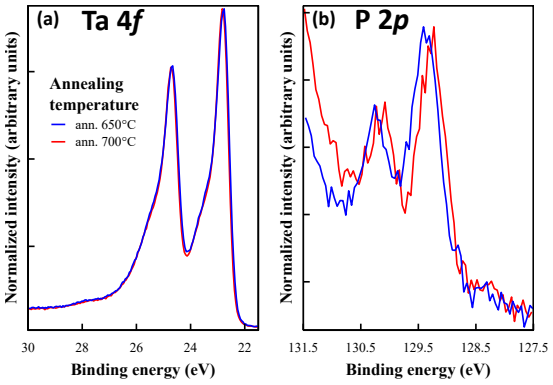

Figure S4: (a) Ta $4f$ CLs and (b) P $2p$ CLs measured by XPS on two samples grown at 250°C and annealed at 650 or 700°C.

Sample	Growth conditions	Se/Ta ratio
1	250°C ann. 650°C	1.99
2	250°C ann. 650°C	2.00
3	250°C ann. 650°C	2.02
4	250°C ann. 700°C	1.99

Table S1: Se/Ta atomic ratios calculated from XPS measurements at 25°. Several samples grown at 250°C and annealed at 650°C show the very good reproducibility of the measurement.

The XPS spectra (Fig. S1 (a,b)) seem independent of the annealing temperature. In particular, no additional component at low binding energies appears in the P $2p$ CLs. Only a small shift is noticeable on the P $2p$ CLs which is related to a slight difference in the substrate doping (7×10^{17} and 3×10^{16} cm^{-3} for the sample annealed at 650 and 700°C respectively, both n-type). The composition of the layer annealed at 700°C (Table S1) also perfectly matches those annealed at 650°C.

Supplementary 5 XPS 5MLs $TaSe_2$ as-grown

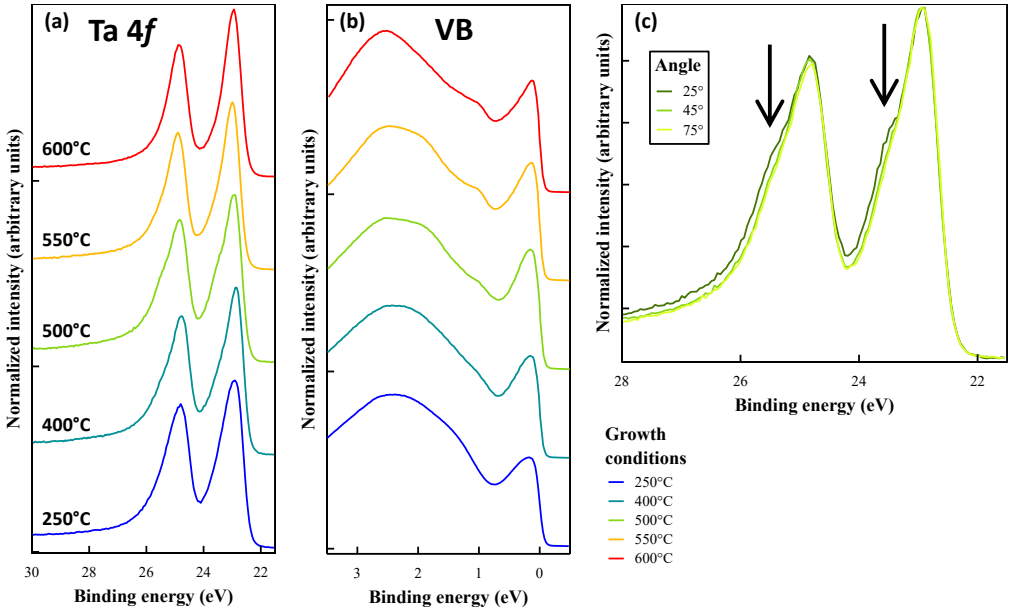

Figure S5: (a) Ta $4f$ CLs measured by XPS at an emission angle of 45°. (b) Valence band measured by UPS using He I (21.2 eV) photons. (c) Comparison of Ta $4f$ CLs measured by XPS at three different emission angles for the sample grown at 500°C.

By contrast to the $TaSe_2$ monolayers, the Ta $4f$ CLs of the as-grown multilayers seen in Fig. S5 (a) are narrower as grown even at low growth temperature. In addition, the splitting induced by the CDW of the 1T phase is not observed at any growth temperature, which indicates that the 1T phase is not present in substantial amount. This is however less obvious for the valence band (Fig. S5 (b)) which does not exhibit distinctly the characteristics observed in monolayer 1H and 1T-$TaSe_2$. It is worth mentioning that despite the thickness and stacking are known to affect the band structure in few layers $TaSe_2$,[5] some features should be conserved such as the low electron density near E_F in Γ in 2H-$TaSe_2$, as previously reported by UPS on bulk $TaSe_2$.[6] The non-negligible density of states measured near E_F in every as-grown sample may be related to structural disorder, because the RHEED patterns do not present thin streaks, or to the presence of a minority of 1T phase. The latter would be in better agreement with the previous studies, which seemed to detect the 1T phase in multilayers grown at low growth temperature.[7,8] The detection of this minor 1T phase in UPS rather than in XPS can be explained by the greater surface sensitivity of UPS, especially if the 1T phase lies at the top of the stacking as observed in STEM after annealing. Comparing the Ta $4f$ CLs measured at different take-off angles on the sample grown at 500°C (Fig. S5 (c)), it is indeed possible to highlight the presence of a more prominent shoulder at a take-off angle of 25° where XPS is more sensitive to the surface. This can be the signature of a minor fraction of 1T phase, which is difficult to detect in XPS because the second peak of the 1T phase is found at the same binding energy as the shoulder usually attributed to a 2H phase.

Supplementary 6 Ta 4*f* 5MLs $TaSe_2$ 600°C annealed 700°C

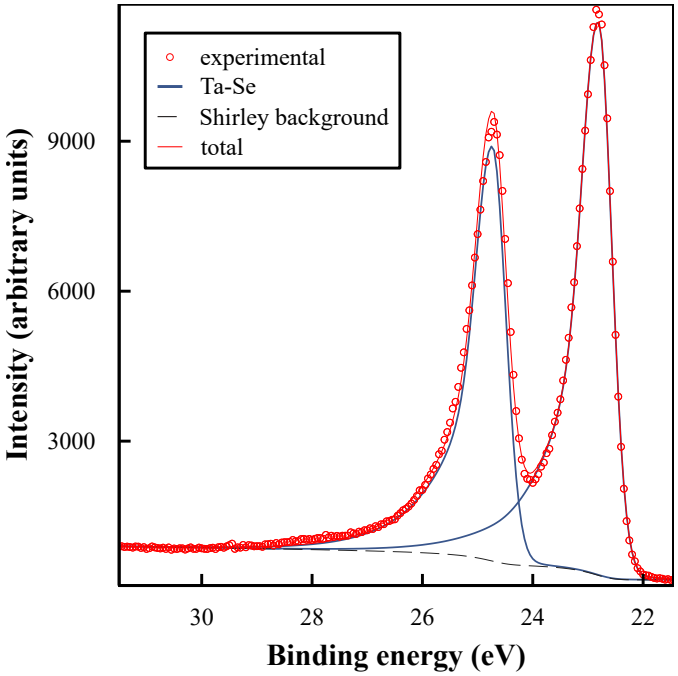

Figure S6: Fit of the Ta 4*f* core levels of a 5ML-thick $TaSe_2$ film grown at 600°C and annealed at 700°C.

In spite of the decrease of the Se/Ta ratio measured in the layer at high growth temperature, no additional component is evidenced at lower binding energy, as it would be expected if metallic Ta clusters were formed. We conclude that the excess Ta atoms are still bonded to Se atoms, possibly in intercalation sites. Though, because the electronegativity of P atoms is relatively close to Se ones, it cannot exclude the presence of Ta-P bonds.

Supplementary 7 P 2*p* CLs 5MLs $TaSe_2$ as-grown

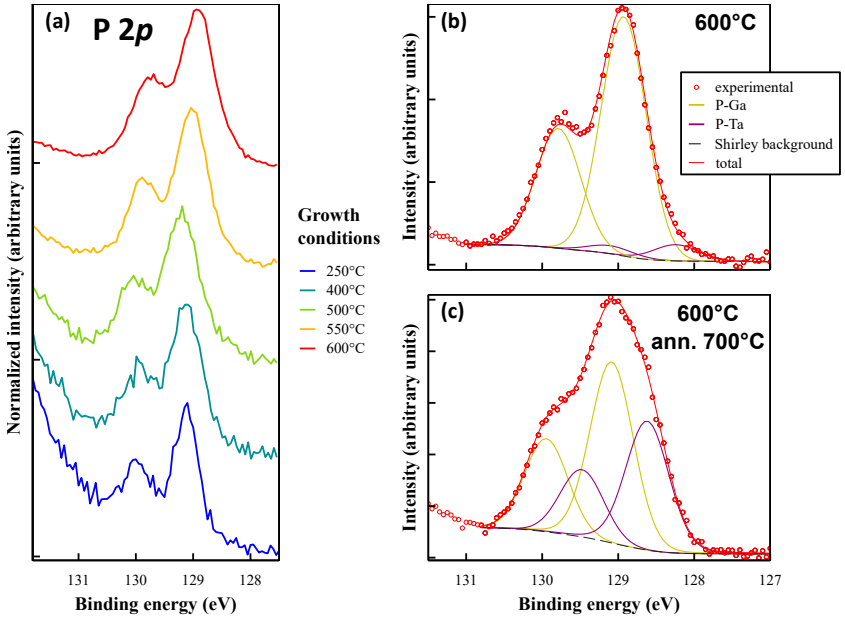

Figure S7: (a) P 2*p* CLs measured on $TaSe_2$ multilayers by XPS at an emission angle of 45° before annealing. (b) Fit of the P 2*p* CLs measured on the sample grown at 600°C before annealing. (c) Fit of the P 2*p* CLs measured on the sample grown at 600°C after annealing at 700°C.

The comparison of the P 2*p* CLs Fig. S7 (a) does not reveal any evidence of a second component. Note that unlike all other samples in Fig. S7 and Fig. 6, the samples prepared at 550°C and 600°C without annealing were grown on p-type substrates which reduces the difference between Ga-P and Ta-P binding energies due to the band bending in the substrate. This make the detection of Ta-P bonds less straightforward so a fit of the P 2*p* CLs in the sample grown at 600°C on p-type GaP is presented before and after annealing respectively in Fig. S7 (b) and S7 (c). If a small component, which is attributed to Ta-P bonds, is detected on the low binding energy side of the as-grown sample, this is significantly less than what is observed for the same sample after annealing. As a conclusion, the Ta-P bonds mostly form during the annealing.

Supplementary 8 Electrical characterization

For the calculation of the resistivity and the measurement uncertainty, a rectangular sample has been used with a width of 2.3 ± 0.1 mm and a length between the inner probes of 1.4 ± 0.2 mm. Its thickness is estimated at 1.9 ± 0.3 nm (3.0 ± 0.5 ML)

Similar results are obtained on other samples using the probes in the square configuration. However, the calculation of the resistivity is less straightforward due the proximity of the sample edges which induces a correction factor between 0.5 and 1[9] (0.75 ± 0.25).

Growth conditions	Intensity (mA)	Voltage (V)	Thickness (nm)	Geometry	Resistivity (μΩ.m)
250°C ann. 650°C	0.1	0.037	1.9 ± 0.3	Line	1.8 ± 0.7
250°C ann. 650°C	1	0.179	1.9 ± 0.3	Square	2.4 ± 1.3
400°C ann. 650°C	1	0.091	2.4 ± 0.3	Square	1.5 ± 0.8
500°C ann. 700°C	1	0.149	2.7 ± 0.3	Square	2.8 ± 1.4

Table S2: Resistivities calculated for $TaSe_2$ multilayers grown at different temperatures. In the square configuration, the voltage is the mean of four measurements corresponding to different contact permutations.

Supplementary 9 Work function measurement

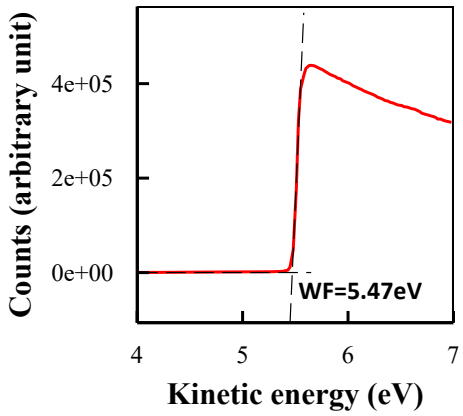

Figure S8: Extraction of the work function from the secondary electron cutoff in the UPS spectrum (hν=21.2 eV) of a 5ML-thick $TaSe_2$ film grown at 500°C and annealed at 650°C.

Supplementary 10 Oxidation

A $TaSe_2$ layer grown at 250°C, annealed at 650°C and left in air for 90 hours (3.7 days) was measured in XPS at different take-off angles. The Ta 4*f* CLs shown in Fig. S9 exhibit a decrease of the intensity of Ta-Se bonds compared to Ta-O at large angles when the analyzed depth is reduced. It leads to the conclusion that the layer is mostly oxidized near the surface.

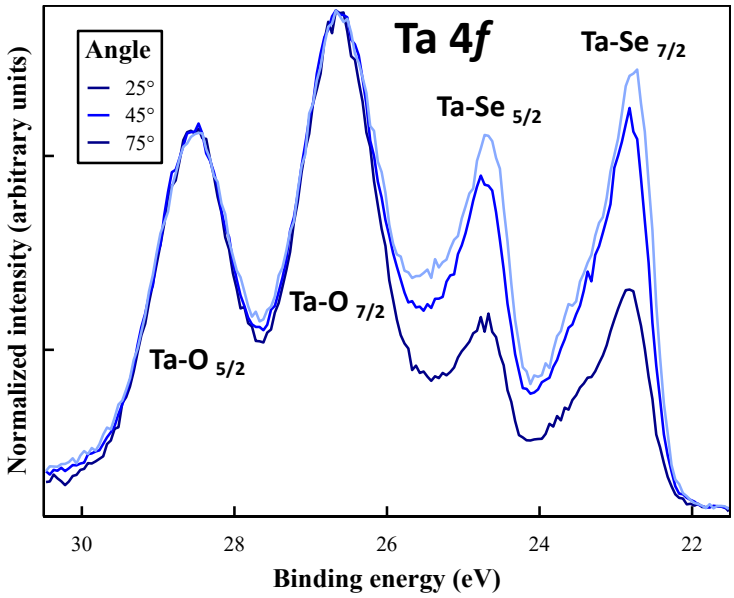

Figure S9: Ta 4*f* CLs of a $TaSe_2$ layer grown at 250°C and annealed at 650°C measured at different take-off angles after 3 days in air.

References

(1) Moeini, B.; Linford, M. R.; Fairley, N.; Barlow, A.; Cumpson, P., et al. *Surface and Interface Analysis* **2022**, *54*, 67–77.

(2) Doniach, S.; Sunjic, M. *Journal of Physics C: Solid State Physics* **1970**, *3*, 285.

(3) Horiba, K.; Ono, K.; Oh, J. H.; Kihara, T.; Nakazono, S., et al. *Physical Review B* **2002**, *66*, 073106.

(4) Brauer, H. E.; Starnberg, H. I.; Holleboom, L. J.; Hughes, H. P.; Strocov, V. N. *Journal of Physics: Condensed Matter* **2001**, *13*, 9879.

(5) Yan, J.-A.; Cruz, M. A. D.; Cook, B.; Varga, K. *Scientific reports* **2015**, *5*, 1–13.

(6) Jakovidis, G.; Riley, J. D.; Leckey, R. C. G. *Journal of electron spectroscopy and related phenomena* **1992**, *61*, 19–26.

(7) Shimada, T.; Ohuchi, F. S.; Parkinson, B. A. *MRS Online Proceedings Library (OPL)* **1991**, *230*, 231–236.

(8) Shimada, T.; Nishikawa, H.; Koma, A.; Furukawa, Y.; Arakawa, E., et al. *Surface science* **1996**, *369*, 379–384.

(9) Miccoli, I.; Edler, F.; Pfnür, H.; Tegenkamp, C. *Journal of Physics: Condensed Matter* **2015**, *27*, 223201.